Design of high precision dynamic star emulator by two-beam combination method

Abstract: In order to improve the simulation accuracy of the precision dynamic star emulator to the infinite sky to meet the needs of the ground calibration of the star sensor and meet the different needs of the design of the high-precision dynamic star emulator, a method for designing the initial structure of the high-precision dynamic star emulator is proposed. Firstly, the technical specifications of the star emulator are obtained by combining the requirements of the ground test of the star sensor, and then the design parameters of the projection optical system are calculated. According to the technical specifications, the light group 1 and the light group 2 are designed, and then the two light groups are combined into a new light group as the required. As the initial structure, the design optimization is carried out through the CODE V software, and the distortion of the system is mainly controlled. The final design result is: the field of view is 22 °, the focal length is 37.34mm, the pupil distance is 40mm, the distortion in the full field of view is less than 0.05%, and the MTF is close to the diffraction limit.

Key words: star emulator; projection optical system; star sensor; optical design; combined light group.

1 Introduction

The star sensor can measure the brightness and spatial coordinates of the star, and obtain its attitude information by comparing it with the observation data in the star catalog. The star sensor is such a device, which can complete the identification of the star map and

accurately locate the attitude of the aircraft [1]. Due to the small opening angle between the stars, the images of the stars are taken in a vacuum environment, and the right ascension and declination of the stars are accurate when shooting. Therefore, the attitude angle accuracy of the calculated star sensor can reach the order of seconds, which is the most accurate one among various attitude measurements at present. In the process of developing the star sensor, there needs to be a device that can simulate the real state of the starry sky in the laboratory, and this device is the star emulator [24,25]. The stellar emulator is mainly used to simulate the star points. In order to meet the testing requirements and ensure the connection between the exit pupil of the projection system and the entrance pupil of the system to be inspected, a scheme for designing the dynamic star emulator optical system is proposed [26,27]. This paper mainly designs and optimizes the projection optical system to ensure that the optical system has good imaging quality, and provides optical support for the high-precision simulation of the infinite star field [2-4].

When using CODE-V to optimize the optical system, the appropriate initial structure is usually selected in CODE-V's patented lens library according to parameters such as field of view, F number and lens type for optimization. However, the initial structure found by this method sometimes does not meet all the requirements very well. Often, while ensuring the entrance pupil distance and entrance pupil diameter, the lens cannot be guaranteed to have good imaging quality [5]. This paper proposes a method for designing the initial structure. Through calculation, two light groups that meet some requirements can be obtained, and then the two light groups are combined. The obtained new light group can meet the requirements of relevant initial parameters, and at the same time ensure that the lens has good imaging quality [28,29]. Through the initial parameters, we can calculate the relevant parameters of the two light groups separately, find the relationship between the relevant parameters of the two light groups, and then splice together to form a new light group, optimize the new light group, and obtain a high-precision dynamic star emulator.

2 Working principle and composition of dynamic star emulator

The composition of the dynamic star emulator system is shown in Figure 1.

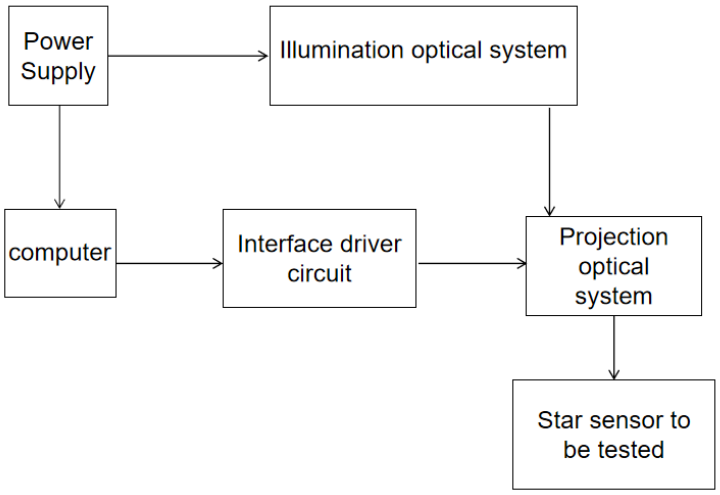

Figure 1 Composition of dynamic star emulator system

Among them, the power supply is mainly responsible for the power supply of each electrical equipment in the ground simulation and testing environment; the main control computer is responsible for searching the built-in star library according to the preset orbit, attitude and other data of the star sensor and generating star coordinates, brightness and other star map data in the field of view of the star sensor that meet the requirements. The star map data is transmitted to the star map display device through the interface driving circuit, and the star map image is generated on the surface of the star map display device [6]; the lighting optical system is responsible for generating spectra, divergence angles, uniformity and other indicators that meet the needs of the light, and the light is irradiated on the imaging surface of the star map display device to generate a high-brightness image; The image is corrected by the projection optical system, converted into a parallel light image that meets the requirements and projected to the star sensor, completing the closed-loop experiment of the ground simulation test [7].

3 Design of Projection Optical System

3.1 Optical system parameters

In the dynamic star emulator, the projection optical system is connected with the system to be inspected, so the quality of the projected image directly determines the test accuracy of the star emulator. In the design of the optical system, in order to prevent the light signal of the star emulator from being transmitted to the star sensor from having a large loss, under the premise of satisfying the pupil connection principle, it is necessary to ensure that the exit pupil of the star emulator is larger than the entrance pupil of the star sensor [8-10]. Since the dynamic star emulator is the ground calibration device of the star sensor, according to the testing requirements of the star sensor, the star emulator designed in this paper has a pupil distance of 40mm, an exit pupil diameter of 10mm, a field of view of 22 °, and an operating wavelength of 0.4-0.7 μm. The DMD contains 1920 × 1080 pixels, and the single pixel size is 7.56 μm. According to Nyquist's law, the modulation transfer function should be γ Nyquist = 1/(2 × 7.56 μm) = 66lp/mm when evaluating the optical system. According to the above given parameters, the focal length of the projection optical system and the corresponding F number can be calculated.

The focal length of the projection optical system is calculated from the above parameters, and the corresponding F number is:

$$f = \frac{h}{tan\omega} = \frac{15.09}{tan22^{\circ}} = 37.34\text{mm}$$

$$F = \frac{f}{D} = 3.735$$

Where h is the image plane height, ω is the field of view of the projection optical system, and D is the exit pupil aperture.

According to the above analysis, the parameters of the projection optical system are shown in Table 1.

Table 1 Design parameters of star emulator projection optical system

system parameters	numerical value
working band	0.4μm-0.7μm

exit pupil diameter	10mm
out-pupil distance	40mm
Field of view	22°
focal length	37.35mm
F number	3.735
MTF@66lp/mm energy concentration	0.3≥80%@15μm
distortion	＜0.1%

3.2 Optical system design process

According to the calculation formulas of the optical system such as the object-image relationship and the vertical axis magnification, the parameters of the two optical systems in the front group and the back group can be obtained [12]。

$$\beta = \frac{l'}{l} = \frac{y'}{y}$$

$$\frac{1}{l} + \frac{1}{l'} = \frac{1}{f2}$$

$$\frac{1}{f1} + \frac{1}{f2} - \frac{f1 + f2 + d}{f1 * f2} = \frac{1}{f}$$

$$l = f2 + d$$

Wherein the combined optical system focal length: f; front group optical system focal length: f1; rear group optical system focal length: f2; object height: y; image height: y first derivative; object distance: l; image distance: l first derivative; vertical axis magnification: Beta distance between the two light groups: d.

The main technical parameters are shown in Table 2.

Table 2 Design parameters of star emulator projection optical system

system parameters	numerical value
f	37.34mm
f1	30mm
f2	49.43mm
F1	1.17
F2	1.41

l	89.17mm
l'	110.95mm
β	1.24
d	39.72mm

At present, there are two commonly used methods to determine the initial structure: analytical method and scaling method.

Analytical method: This method is based on geometric aberration theory and constructs the initial structure through primary aberration theory. It allows designers to directly calculate the curvature, spacing, thickness, and material parameters of the lens according to the required optical performance indicators (such as focal length, aperture number, field of view, etc.). The advantage of analytical method is that it can quickly obtain a starting design scheme that theoretically meets the basic requirements, but this scheme may need further optimization to reduce aberrations and achieve higher imaging quality.

Zoom method: This method usually involves referring to existing patented lenses or known lens structures and scaling and modifying these structures according to new technical specifications. Designers analyze the imaging quality of existing lenses and then adapt them to new design requirements by adjusting their size, shape, and glass materials. Zoom method relies on the experience and results of existing designs and often requires repeated optimization and iteration to ensure that the final design meets specific technical specifications [13].

The text is designed using the zoom method, and the appropriate lens structure is selected in the COVE V patent lens library according to the calculated focal length, F number and field of view. The optical system optical path diagrams of the selected front and rear groups are shown in Figure 2 and Figure 3, and the combined optical system optical path diagram is shown in Figure 4.

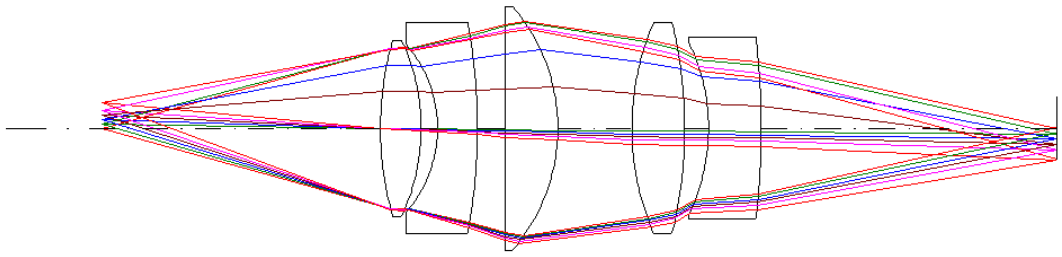

Figure 2 Optical path diagram of the front group optical system

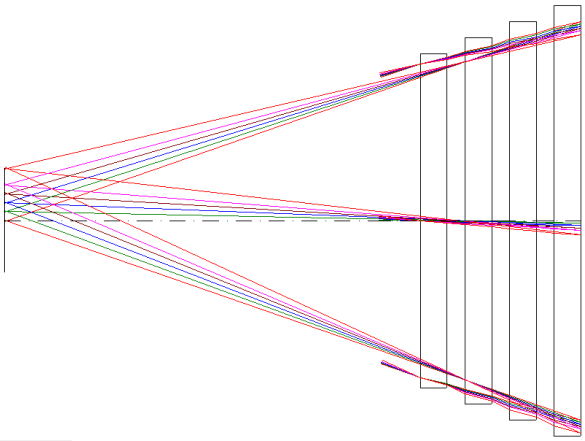

Figure 3 Optical path diagram of the rear group optical system

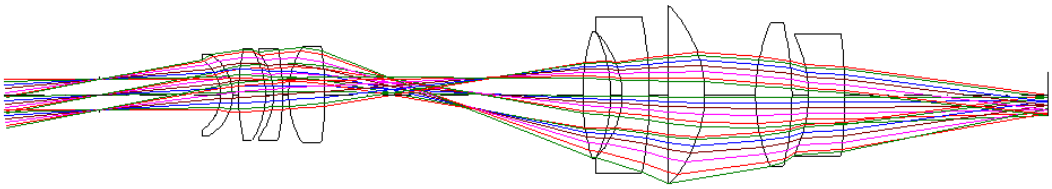

Figure 4 Optical path diagram of the combined optical system

3.3 Optical System Design Results

Based on the CODE V optical design platform, the optimization design is completed with the focal length, back focus, incident angle, distortion, and overall length of the optical system as constraint parameters. The obtained optical system optical path diagram is shown in Figure 5.

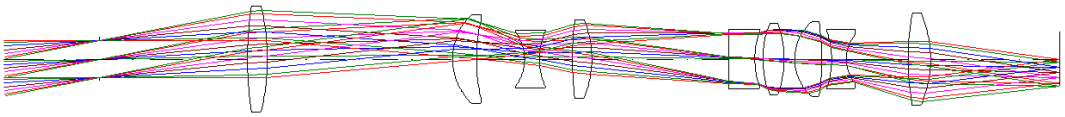

Fig. 5 Optical path diagram of projection optical system

According to the design results, the focal length of the optical system is 37.34mm, the back focal length is 35mm, the exit pupil diameter is φ 10mm, and the exit pupil distance is 40mm. There are 9 lenses in total, of which the first lens has the largest aperture, which is φ 26.28mm. The total length of the optical system is 260mm.

4 Analysis of Projection Optical System

4.1 image quality analysis

Point plot, MTF curve and distortion are commonly used in image quality evaluation of optical systems. In this paper, CODE V software is used to evaluate the image quality of optical systems.

4.1.1 dot plot

The dot plot shows the distribution of light spots on the image plane of light passing through different parts of the system from object points. The size and shape of these light spots can reflect the aberration of the system.

The distribution state of a dot plot can be expressed by two quantities: the geometric maximum radius value and the root mean square RMS radius value. The geometric maximum radius value is the distance from the intersection point of the reference ray on the image plane to the farthest light intersection point, that is, the radius of the largest circle containing all rays centered on the intersection point of the reference ray. It only reflects the maximum value of aberration and cannot reflect the degree of concentration of light energy. The root mean square radius is the root mean square of the distance between each light intersection point and the reference light intersection point on the image plane, reflecting the concentration of light energy and better reflecting the imaging quality of the system.

If the light spots in the dot plot are closely concentrated, it indicates that the aberration of the system is small; if the light spot distribution is more scattered, it indicates that there is a large aberration [14].

The distribution of light and image plane intersections in several fields of view from 0 to 1 is shown in Figure 6.

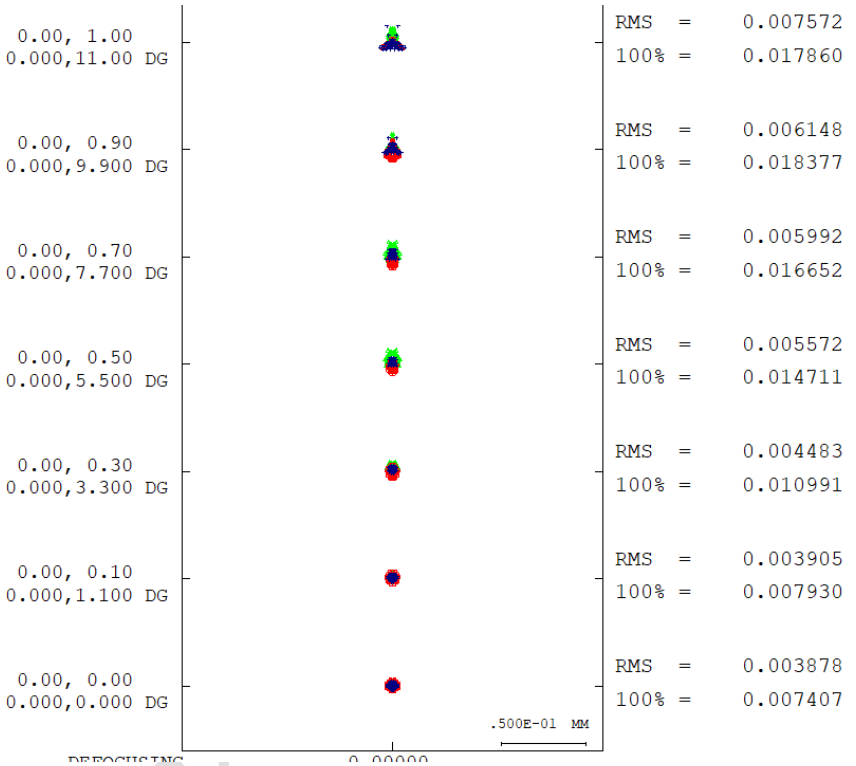

Figure 6 Point diagram of the optical system

It can be seen that the RMS radius of the maximum field of view is 7.57 μm, indicating that the energy concentration and symmetry of the projection optical system are good, the center position of the light spot is stable, and the imaging quality is good.

4.1.2 Field curvature and distortion

In optical systems, field curvature shows that the imaging surface at different positions in the field of view is not an ideal plane, but a curved surface. This means that on a specific focal plane, only the central area or a specific area can be clearly imaged, while other areas become blurred. This phenomenon is particularly evident in optical systems with a wide field of view. For dynamic star emulators, the presence of field curvature may lead to inaccurate star positioning and blurred star maps.

Distortion is a ubiquitous aberration in optical systems that affects the position of the star point on the imaging plane, but does not affect its clarity. In a dynamic star emulator, distortion is caused by a difference between the actual height of the intersection of the main ray and the Gaussian image plane, the first derivative of Y z, and the first derivative of the ideal height y. This difference is usually expressed as the first derivative of Delta uppercase Y z, and is defined as follows [15-16].

$$\delta Yz' = Yz' - y'$$

Relative distortion refers to the percentage of the image height difference and the ideal height, which is commonly expressed by q ′ and is defined as follows.

$$q' = \frac{\delta Yz'}{y'} \times 100\% = \frac{Yz' - y'}{y'} \times 100\%$$

For a dynamic star emulator, distortion can cause the image position of the star point to deviate from its ideal position.

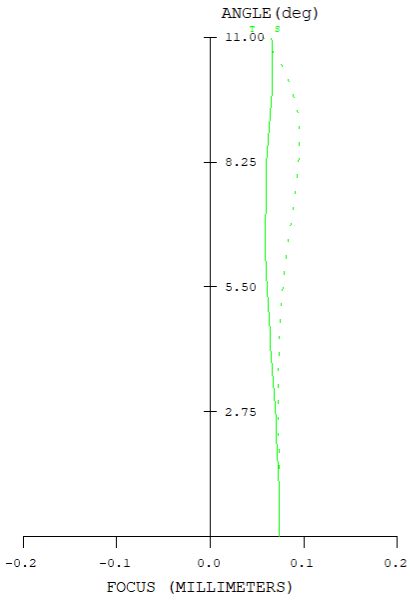

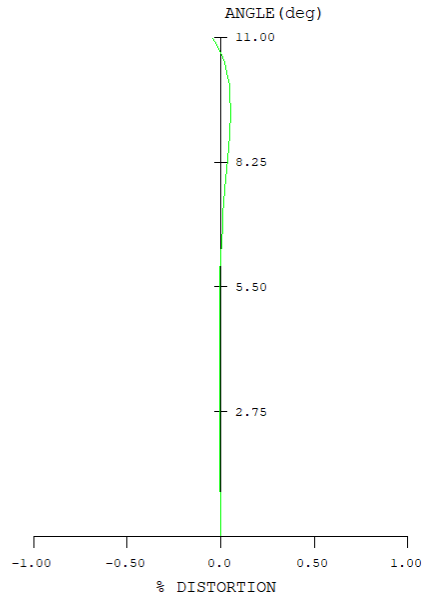

RELATIVE FIELD HEIGHT	ANGLE (DEG)	X-FOCUS AT THE IMAGE SURFACE	Y-FOCUS AT THE IMAGE SURFACE	X-FOCUS (DISPLACED BY 0.000000)	Y-FOCUS (DISPLACED BY 0.000000)	DISTORTION (PER CENT)
0.00	0.00	0.074035	0.074035	0.074035	0.074035	0.00000
0.10	1.10	0.073247	0.073763	0.073247	0.073763	-0.00108
0.20	2.20	0.071013	0.073192	0.071013	0.073192	-0.00390
0.30	3.30	0.067729	0.073026	0.067729	0.073026	-0.00712
0.40	4.40	0.064036	0.074270	0.064036	0.074270	-0.00858
0.50	5.50	0.060783	0.077898	0.060783	0.077898	-0.00544
0.60	6.60	0.058935	0.084206	0.058935	0.084206	0.00513
0.70	7.70	0.059361	0.091715	0.059361	0.091715	0.02413
0.80	8.80	0.062333	0.095608	0.062333	0.095608	0.04600
0.90	9.90	0.066354	0.086722	0.066354	0.086722	0.04662
1.00	11.00	0.065122	0.057095	0.065122	0.057095	-0.04696

Figure 7 Field curvature and distortion

As shown in Figure 7, the left side represents the field curvature of the optical system, and the right side represents the distortion in percentage. The field curvature of the projection optical system designed in this paper is less than 38.5 μm, and the distortion of the full field of view is less than 0.05%. Meet the technical specifications of dynamic star emulators.

4.1.3 optical transfer function curve

MTF (Modulation Transfer Function) is a function that describes the ability of an optical system to transmit different spatial frequencies of an object. It is usually a value between 0 and 1 that represents the degree of retention of contrast at different frequencies. MTF is mainly composed of two parts: resolution and contrast. Resolution reflects the ability of an optical system to distinguish details of an object, usually expressed in line pairs per millimeter (lp/mm). Contrast, in turn, indicates the degree of difference between light and dark in the light and dark parts. An MTF close to the diffraction limit means that the system is able to simulate the star map more realistically, maintaining a high imaging quality. Through MTF, the imaging performance of the optical system such as the ability to transfer details, layers and contours of the object can be comprehensively evaluated. Among them, the high frequency part reflects the detail transfer ability, the intermediate frequency part reflects the level transfer ability, and the low frequency part reflects the contour transfer ability [17].

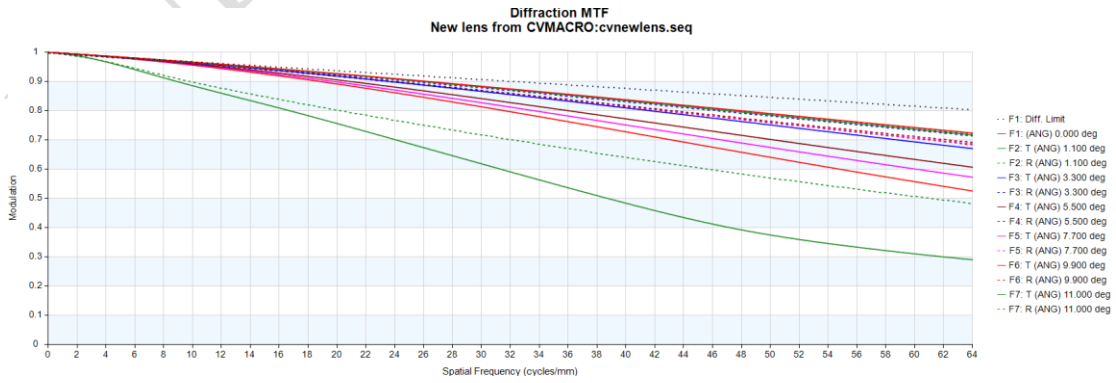

Fig. 8 Optical transfer function curve of projection optical system

As shown in Figure 8, the abscissa represents the spatial frequency in line pairs per

millimeter (lp/mm), which represents the scale of the smallest detail that can be resolved in an image. The ordinate represents the contrast, which ranges from 0 to 1, where 1 represents the maximum possible contrast, which is the case where black and white are most distinct. Ideally, the MTF curve will stick close to the top of the ordinate, which means the system maintains the highest contrast at all spatial frequencies. However, practical optical systems are often unable to do this. The MTF in the figure is greater than 0.3 in the full field of view at 66lp/mm, and greater than 0.5 in the 0.9 field of view, which means that at a spatial frequency of 66 line pairs per millimeter, the system can transfer almost 50% of the contrast, meeting the requirements of the dynamic star emulator star map display.

4.2 tolerance analysis

The projection optical system is an imaging optical system. Since the distortion has a significant impact on the position simulation accuracy of the dynamic star emulator, in the tolerance analysis, in addition to analyzing the influence of the tolerance on the MTF, it is also necessary to analyze the influence on the distortion [18].

In practical work, the tolerances of optical and mechanical components and optical glass are determined according to the generally achievable machining accuracy and the material characteristics provided by optical glass manufacturers [19], and the results are shown in Table 3.

Table 3 Material properties

material properties	request
Δ nd	1A
Δvd	1A
optical uniformity	1
light absorption coefficient	2
birefringence	2
stripe	1B
Bubble degree	1C

Table 4 CODE V tolerance allocation

tolerance	value
DLF Irregular aperture number	2
DLR - Radius Increment (Lens Unit)	Class A template (0.0005 * R)
DLT - Thickness increment (lens unit)	±0.01
DLN - Refractive Index Increment	0.0005
CYD CYN surface irregularity	0.05
DLA DLB Tilt Tolerance (radians)	0.003
DLX DLY off-axis tolerance	0.001

MTF-based tolerance analysis is designed to assess the effect of tolerance changes for individual lenses in an optical system on the overall MTF in order to determine which lenses' tolerances need to be more tightly controlled. Figure 9 shows the MTF tolerance analysis result curves at different fields of view (0, 0.1, 0.3, 0.5, 0.7, 0.9, and full field of view). MTF decrease values with a confidence level of 99.9% for each field of view. This means that there is a 99.9% confidence that, within these tolerances, the MTF decrease for the system will not exceed the values given in the table.

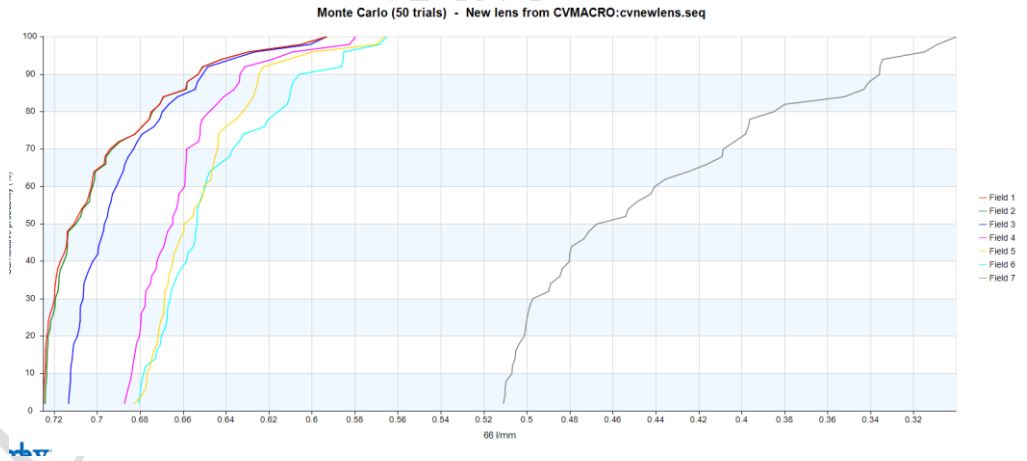

Figure 9 Effect of tolerances on MTF

The MTF results are shown in Table 5. In different fields of view, the maximum decrease in MTF is 0.17, indicating that the set tolerance range meets the requirements.

Table 5 MTF decrease at 99.9% confidence level 0

Field of view	MTF decline
0ω	-0.121557

0.3ω	-0.111223
0.5ω	-0.099630
0.7ω	-0.107377
0.9ω	-0.110685
1.0ω	-0.174443

Geometric energy concentration is used to evaluate the energy diffusion of a single pixel object point in an optical system after imaging under different fields of view. Ideally, the energy diffusion of each object point formed by the image point after imaging through the optical system is concentrated in one pixel size. However, due to aberrations in practical optical systems, the energy of the imaged image point will spread inside and outside the pixel size range, forming diffraction spots.

The center energy degree (S. D) is a parameter that measures the ratio of the center energy of the actual imaged diffraction spot to the ideal imaged diffraction spot. The geometric energy concentration curve shown in Figure 10 shows the 80% energy concentration at different fields of view [20].

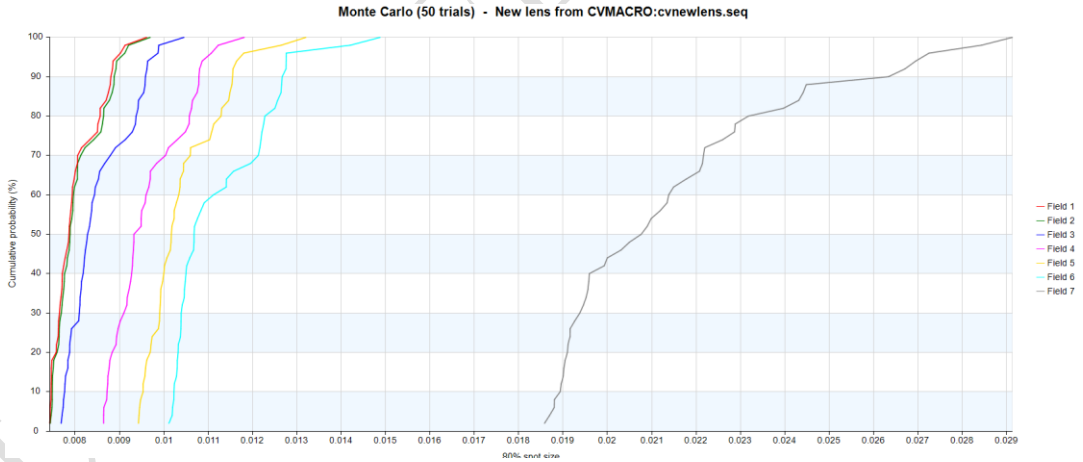

Figure 10 Effect of tolerance on 80% energy concentration

According to the Stoller criterion, S. D $\geqslant$ 0.8, the imaging quality of the optical system meets the requirements for energy concentration.

Table 6 80% surround energy at confidence level

	Field of view size	Initial 80% energy distribution	99.9% added value (mm)	Analyzed diameter (mm)

		diameter (mm)		
1	0°	0.007815	0.001775	0.00959
2	6.6°	0.007867	0.001803	0.00967
3	11°	0.008356	0.002071	0.010427
4	15.4°	0.009503	0.002282	0.011785
5	19.8°	0.010140	0.003035	0.013175
6	22°	0.010444	0.004398	0.014842

As can be seen from Table 6, the Monte Carlo analysis shows that the geometric energy concentration curves of each field of view are consistent, and 80% of the surrounding energy distribution of each field of view is located within 14.84 μm in diameter at 99.9% confidence level, indicating that the energy concentration is good and meets the requirements of use.

5 conclusion

The star sensor is one of the most important sensors for spacecraft. Stability, detection accuracy and other indicators are crucial to determine the pose of the entire spacecraft. As a ground test equipment for star sensors, the requirements for star map generation accuracy and dynamics of star dynamic emulators are also getting higher and higher. This paper studies the dynamic star emulator projection optical system based on DMD. The specific work is as follows:

(1) A new method for calculating the initial structure of the lens is proposed.

(2) The proposed method is verified, the dynamic star emulator commonly used in the market is analyzed, and the commonly used parameters are selected as the parameters of this emulator design.

(3) The projection optical system and its important parameters are analyzed, and the projection optical system is designed according to the design process. The design results of the projection optical system are analyzed and evaluated. The MTF (66lp/mm) of the optical system is > 0.3, the RMS radius of the maximum field of view is 7.57 μm, and the distortion of the full field of view is less than 0.05%. The results show that the imaging

quality meets the design requirements.

(4) The tolerance analysis of the designed projection optical system shows that in different fields of view, the maximum decrease of MTF is 0.17, and the geometric energy concentration curves of each field of view are consistent. At 99.9% confidence level, 80% of the surrounding energy of each field of view is located within 14.84 μm in diameter, indicating that the energy concentration is good and meets the requirements of use.

Disclaimer (Artificial intelligence)

Author(s) hereby declare that NO generative AI technologies such as Large Language Models (ChatGPT, COPILOT, etc.) and text-to-image generators have been used during the writing or editing of this manuscript.

References

[1] Ma Xuemei, Xue Huifeng, Yuan Jianhua, et al. The development trend of aerospace technology research in major aerospace countries - scientometric analysis based on Web of Science database [J]. Information Engineering, 2017,3 (4): 087-098.

[2] Li Jie. Research on key technology of APS star sensor [D]. Graduate School of Chinese Academy of Sciences (Changchun Institute of Optics, Fine Mechanics and Physics), 2005.

[3] Li Chengzhi. Breakthrough Development of China Aerospace Technology [J]. Journal of Chinese Academy of Sciences, 2019,34 (9): 1014-1027.

[4] Chen Na. Research on high-precision magnitude simulation technology of dynamic star emulator [D]. Changchun University of Science and Technology [2024-04-06].

[5] Hu Yining. Research on small dynamic star emulator technology [D]. Graduate School of Chinese Academy of Sciences (Changchun Institute of Optics, Fine Mechanics and Physics), 2010.

[6] Liyan L, Luping X, Hua Z. An Autonomous Star Identification Algorithm Based on One Di- mensional Vector Pattern for Star Sensors [J]. Sensors, 2015, 15 (7): 16412-16429.

[7] Zhang L, Yang H, Lu H, et al. Cubature Kalman filtering for relative spacecraft attitude and position estimation [J]. Acta Astronautica, 2014, 105 (1): 254-264.

[8] Xiong Kuiyun. Research on Earth attitude control method of low-orbit microsatellites [D]. Shenyang University of Technology, 2017.

[9] ZHANG Hua. Research on key technologies of high-precision dual-field star sensor [D]. Huazhong University of Science and Technology, 2011.

[10] Hao Yuncai. Progress and Application of Space Optical Sensor Technology [J]. Space Control Technology and Application, 2017, 43 (04): 9-18.

[11] Guangtan Xu, Deren Gong, Dengping Duan. Recursive optimal linear attitude estimator based on star sensor and gyro [J]. Aerospace Systems, 2021.

[12] Mona Zahednamazi, Alireza Toloei, Reza Ghasemi. Different types of star identification algorithms for satellite attitude determination using star sensors [J]. Aerospace Systems, 2021, 4 (4).

[13] Wang Hongrui, Li Huidian, Fang Wei. Application and development of aerospace solar sensors [J]. China Optics, 2013, 6 (04): 481-489.

[14] Rogers D G, Schwinger R M, Kaidy T J, et al. Autonomous star tracker performance [J]. Acta Astronautica, 2009, 65 (1-2): 61-74.

[15] Surrow B. The STAR Forward GEM Tracker [J]. Nuclear Instruments and Methods in Physics Research Section A: Accelerators, Spectrometers, Detectors and Associated Equipment, 2019, 617 (1-3): 196-198.

[16] Wang Hongtao, Luo Changzhou, Wang Yu, et al. Analysis of dynamic angle measurement of missile-borne star sensor [J]. Modern Defense Technology, 2010, 38 (01): 37-41.

[17] Chubei S M, Koval'chuk V L, Kholodova I S, et al.Star sensor for independent navigation in deep space [J]. Journal of Optical Technology, 2007, 74 (2): 107-114.

[18] Zeng Fen, Liu Jinguo, Zuo Yang, et al. Attitude determination method based on multi-field star sensor [J]. Computer Measurement and Control, 2015, 23 (02): 548-550.

[19]LIU Yaping, LI Juan, ZHANG Hong. Design and calibration of star emulator [J]. Infrared and Laser Engineering, 2006, (S1): 331-334.

[20]Liu Shi, Zhang Guoyu, Sun Gaofei, et al. Design of dynamic star emulator based on LCOS splicing technology [J]. Chinese Journal of Space Science, 2013, 33 (02): 200-206.

[21]Xu Honggang, Han Bing, Li Manli, Ma Hongtao, Zhang Pengyu, Ju Dehan. Design and verification of high-precision large-field multi-star emulator [J]. China Optics, 2020, 13 (06): 1343-1351.

[22]Chen Na, Wang Lingyun, Li Guangqian, Cui He, Zhang Runze. Design of collimating optical system for static star emulator [J]. Journal of Changchun University of Science and Technology (Natural Science Edition), 2019, 42 (05): 23-26.

[23]Wang Shiran, Wang Lingyun, Zheng Ru et al. Design of collimating optical system for static star emulator with long pupil distance [J]. Journal of Changchun University of Science and Technology (Natural Science Edition), 2023,46 (03)

[24]Zhu H, He S, Wang X, Qin C, Li L, Sun X. Design and Testing of a Simulator for Micro-Vibration Testing of Star Sensor. Micromachines. 2023 Aug 22;14(9):1652.

[25]Li P, Zhong S, Lv Z, Mou W. Joint Optimization Method for Simulation Parameters and Hardware Latency in High-Precision Navigation Channel Emulators. In2024 International Conference on Ubiquitous Communication (Ucom) 2024 Jul 5 (pp. 102-106). IEEE.

[26]Sun T, Xing F, You Z. Optical system error analysis and calibration method of high-accuracy star trackers. Sensors. 2013 Apr 8;13(4):4598-623.

[27]Heitmann K, Lawrence E, Kwan J, Habib S, Higdon D. The coyote universe extended: precision emulation of the matter power spectrum. The Astrophysical Journal. 2013 Dec 13;780(1):111.

[28]Kao M, Eller D. Multiconfiguration Kalman filter design for high-performance GPS navigation. IEEE Transactions on Automatic Control. 1983 Mar;28(3):304-14.

[29]Qimeng C, Guoyu Z, Lingyun W, Zhihai W, Xiangyang S. Test equipment design of

high precision star sensor. Infrared and Laser Engineering. 2014 Jul 25;43(7):2234-9.